





Observation of terahertz second harmonic generation from Dirac surface states in the topological insulator Bi_2Se_3

Jonathan Stensberg ¹, Xingyue Han,¹ Zhuoliang Ni,¹ Xiong Yao,² Xiaoyu Yuan ², Debarghya Mallick,² Akshat Gandhi ², Seongshik Oh,² and Liang Wu ^{1,*}

¹*Department of Physics and Astronomy, University of Pennsylvania, Philadelphia, Pennsylvania 19104, U.S.A.*

²*Department of Physics and Astronomy, Rutgers, The State University of New Jersey, Piscataway, New Jersey 08854, U.S.A.*



(Received 12 January 2023; revised 19 September 2023; accepted 21 May 2024; published 7 June 2024)

We report the observation of second harmonic generation with high conversion efficiency $\sim 0.005\%$ in the terahertz regime from thin films of the topological insulator Bi_2Se_3 that exhibits the linear photogalvanic effect, measured via time-domain terahertz nonlinear spectroscopy and terahertz emission, respectively. As neither phenomena is observable from topologically trivial In-doped Bi_2Se_3 , and since no enhancement is observed when subject to band bending, the efficient thickness-independent nonlinear responses are attributable to the Dirac fermions of topological surface states of Bi_2Se_3 . This observation of intrinsic terahertz second harmonic generation in an equilibrium system unlocks the full suite of both even and odd harmonic orders in the terahertz regime and opens new pathways to probing quantum geometry via intraband second-order nonlinear processes. We hope our work will motivate the theoretical development of a full treatment of second harmonic generation for probing the quantum geometry in various inversion-breaking topological and twisted materials.

DOI: [10.1103/PhysRevB.109.245112](https://doi.org/10.1103/PhysRevB.109.245112)

I. INTRODUCTION

Harmonic generation (HG) has been an invaluable nonlinear optical technique since its first demonstration [1] and continues to power recent advances ranging from the imaging of microscopic magnetic domains [2,3] to the development of tabletop sources of extreme ultraviolet and x-ray light for attosecond science [4,5]. Nevertheless, employing HG to study phenomena below ~ 100 meV has been severely impeded by the historical terahertz (THz) gap [6], traditionally $\sim 0.1\text{--}30$ THz (1 THz ≈ 4.1 meV), where technical challenges have impeded the development of intense light sources. Recent progress in intense THz generation [7,8], however, has enabled the first applications of HG to the THz regime. Since its first demonstration [9], THz third harmonic generation (THG) has rapidly become a standard tool for characterizing the Higgs mode [9–13] and other nonlinear optical processes [14–27] in a variety of superconductors [28–35]. Yet more recently, odd-order THz-HG has been reported in doped Si [36–38] and materials hosting Dirac fermions, namely graphene [39–42], Cd_3As_2 [43–45], and the bismuth chalcogenide family of topological insulators [42,46,47]. The latest studies have explored effectively tuning the nonlinear process of THz-HG via gating [40] and metasurfacing [41,42].

Despite these advances, THz-HG remains highly constrained, limited almost exclusively to odd-order low harmonics. The most striking limitation is that even-order THz harmonics (which are only permitted under inversion symmetry breaking) have only been observed in superconductors with a net propagating supercurrent [48,49] that drives the

system out of equilibrium to break inversion symmetry, or in carefully engineered metamaterial devices [50] that artificially break inversion symmetry. Intrinsic even-order THz-HG has never been demonstrated in an equilibrium material. This is a severe impediment to studying quantum materials, as second harmonic generation (SHG) has physically different origins than the commonly studied odd-order harmonics, including conventional asymmetric scattering [51], skew scattering of chiral Bloch fermions [52,53], and quantum geometry [54–56]. In the THz regime, interband transitions are precluded in most systems due to the low energy scale, and scattering contributions are diminished due to the frequency exceeding the scattering rate [57,58], making THz-SHG an ideal probe of the intraband quantum geometry (though a full derivation of intraband SHG from quantum geometry still needs to be developed). As prototypical topological insulators with a centrosymmetric bulk and inversion symmetry-breaking topological surfaces, the bismuth chalcogenides [59–62] provide an ideal platform to probe the intraband quantum geometry of the topological surface state via THz-SHG while intrinsically avoiding the properties of the bulk band. However, previous nonlinear THz studies of the bismuth chalcogenides [42,46,47] failed to observe THz-SHG, despite the ubiquity of surface SHG—and even-order HG in general—in the nonlinear optical response outside of the THz regime [63–69]. Realizing THz-SHG originating from Dirac surface states in the bismuth chalcogenides is therefore a crucial step toward opening a powerful nonlinear pathway to measuring intraband quantum geometry via THz-HG techniques.

Here, we report the observation of THz-SHG from Bi_2Se_3 samples exhibiting the linear photogalvanic effect (LPGE). With LPGE determined by THz emission [70] and THz-SHG

*liangwu@sas.upenn.edu

measured via intense time-domain THz spectroscopy (TDS) [71], thin films of Bi_2Se_3 that display LPGE are found to produce THz-SHG that is highly efficient and independent of the sample thickness. As these phenomena are not observed in topologically trivial In-doped Bi_2Se_3 , and since there is no enhancement observed when samples are subject to band bending, the efficient response is attributable to the Dirac fermions of the topological surface states. We further show that as both LPGE and SHG result from second-order nonlinear processes, both effects originate from unequal populations of twinned domains of the threefold symmetric surface of Bi_2Se_3 , which motivates the future development of techniques to preferentially control the orientation of crystal growth on millimeter scales, particularly for materials that break various symmetries. This observation of intrinsic SHG in the THz regime in an equilibrium system enables the future THz-HG investigation of nonlinear intraband quantum processes via the full suite of harmonic orders, both even and odd.

II. RESULTS AND DISCUSSION

Thin film samples of Bi_2Se_3 are grown via molecular beam epitaxy on *c*-axis Al_2O_3 substrates (10 mm \times 10 mm \times 0.5 mm), following standard growth procedures, utilizing the two-step growth process [72,73]. As each van der Waals unit of Bi_2Se_3 forms a quintuple layer (QL), samples of 16 QL, 32 QL, 64 QL, and 100 QL are grown to form a thickness series (1 QL \approx 1 nm). Band bending can occur at the surface of Bi_2Se_3 [74–76], which introduces an internal electric field E_{int} near the surface and results in an effective $\chi^{(2)}$ for second-order processes of $\chi_{\text{eff}}^{(2)} = \chi_{ijk}^{(2)} + \chi_{ijkl}^{(3)} E_{\text{int}}$ [63,65,77]. Therefore, the samples are capped *in situ* with 50 nm of Se, which greatly mitigates band bending, isolates the intrinsic second-order response, and protects against damage [78]. Finally, as sufficient In-doping suppresses the topological surface states of Bi_2Se_3 while being subject to the same band bending effects [46,60], a Se-capped 100 QL sample of $(\text{Bi}_{0.9}\text{In}_{0.1})_2\text{Se}_3$ is grown to directly discriminate between topological and trivial origins.

The samples of Bi_2Se_3 are evaluated for their room temperature LPGE response by measuring the THz emission [70] of the samples under normal incidence, near infrared (NIR) pumping. When a single domain of Bi_2Se_3 is pumped above the bulk band gap of ~ 0.3 eV, photocurrent current generation moves free carriers across the domain [77,79,80]. These carriers are generated from the so-called shift vector from quantum geometry, and also scatter asymmetrically off of the wedge-shaped potential of the trigonal domains [51,81], yielding a low-frequency LPGE current with directionality defined by the domain orientation and which couples out to free space as a THz pulse. This emitted THz pulse is generated and detected by a THz emission spectrometer depicted schematically in Fig. 1(a) and described in previous works [82,83]. In brief, the sample is pumped over a spot size of order 1 mm by linearly polarized, broadband 1530 nm (0.81 eV), 50 fs pulses with a repetition rate of 1 kHz. A quasisingle cycle THz pulse is emitted from the sample in transmission geometry; collected, collimated, and focused onto a ZnTe crystal by a pair of off-axis parabolic mirrors in $4f$ geometry; and measured via

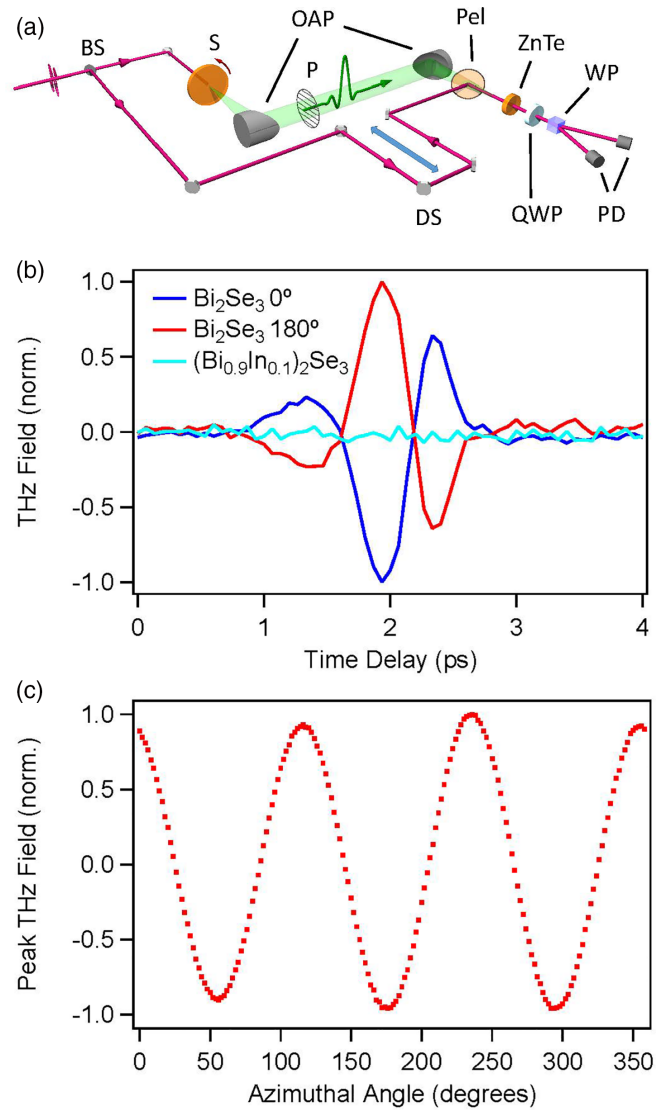


FIG. 1. (a) Schematic of the THz emission spectrometer. The NIR and THz beam paths are depicted in magenta and green, respectively, and the THz beam path is contained in a dry air-purged box. Both sample (S) and polarizer (P) are mounted in rotating stages to enable characterization of the azimuthal angle dependence of the THz emission. Labeled optical elements include beam splitter (BS), pellicle (Pel), ZnTe crystal (ZnTe), quarter wave plate (QWP), Wollaston prism (WP), photodiodes (PD), and delay stage (DS). (b) Normalized electric field profile of the emitted THz pulse from Se-capped 100 QL Bi_2Se_3 and $(\text{Bi}_{0.9}\text{In}_{0.1})_2\text{Se}_3$ obtained by electro-optic sampling mapped in the time domain. (c) The peak normalized electric field as the Bi_2Se_3 azimuthal angle ϕ is rotated.

electro-optic sampling [84]. By varying the optical path length of the NIR probe pulse via the delay stage, the electric field profile of the emitted THz pulse E_{THz} is mapped out in the time domain.

THz emission data is depicted in Figs. 1(b) and 1(c) for typical 100 QL Bi_2Se_3 and $(\text{Bi}_{0.9}\text{In}_{0.1})_2\text{Se}_3$ samples. As shown in 1(b), the $(\text{Bi}_{0.9}\text{In}_{0.1})_2\text{Se}_3$ emits no signal whereas a pronounced quasisingle cycle THz pulse is emitted from the Bi_2Se_3 , the polarity of which changes sign throughout the duration of the pulse when the sample is rotated azimuthally

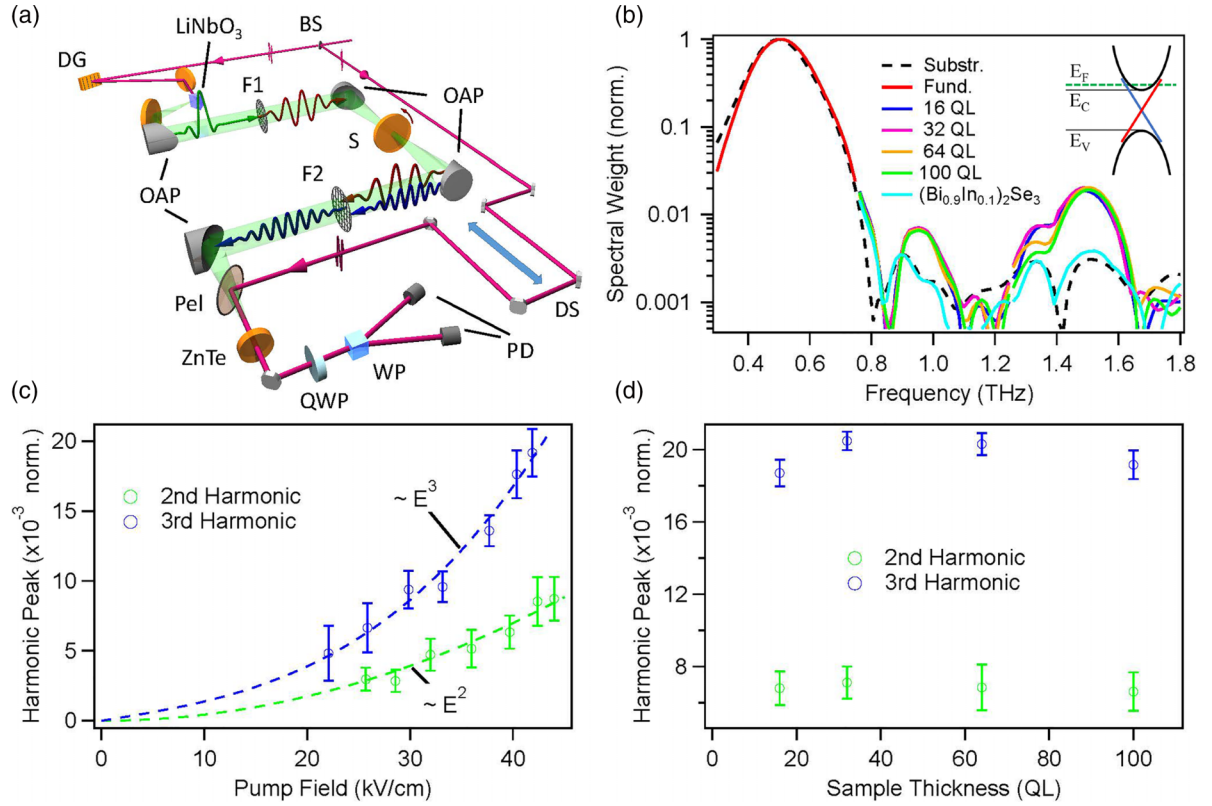


FIG. 2. (a) Schematic of the intense TDTTS system. The NIR and THz beam paths are depicted in magenta and green, respectively, and the THz beam path is contained in a dry air-purged box. Labeled optical elements include sample (S), LiNbO₃ crystal (LiNbO₃), THz filters (F1 and F2), diffraction grating (DG), beam splitter (BS), pelical (Pel), ZnTe crystal (ZnTe), quarter wave plate (QWP), Wollaston prism (WP), photodiodes (PD), and delay stage (DS). (b) Harmonic generation spectra for Se-capped Bi₂Se₃ and (Bi_{0.9}In_{0.1})₂Se₃ samples under a 0.5 THz fundamental pump with respect to a reference substrate. The change between spectra taken with 1.0 THz-specific and 1.5 THz-specific filters are indicated by breaks in the spectra, and the Bi₂Se₃ band structure is sketched with the Fermi level (inset). (c) Bi₂Se₃ peak spectral weight at the second and third harmonic as a function of the peak 0.5 THz pump field E_{pump} , with fits to E_{pump}^2 and E_{pump}^3 , respectively. (d) Peak spectral weight at the second and third harmonics as functions of sample thickness.

by 180 degrees. By tracing out the peak value of E_{THz} as the sample is rotated, as shown in Fig. 1(c), the azimuthal angle dependence clearly follows $E_{THz}^{max} = E_0 \sin(3\phi + \phi_0)$, where E_0 is the peak electric field strength, ϕ is the azimuthal angle, and ϕ_0 is an arbitrary angle difference between the crystalline axes and the laboratory frame for a given sample.

This $\sin(3\phi + \phi_0)$ dependence of the emitted E_{THz} is precisely the azimuthal angle dependence expected for THz emission from a single domain of Bi₂Se₃ due to LPGE under normal incidence [63–66]. LPGE is only permitted in systems that break inversion symmetry [51]. As bulk Bi₂Se₃ is centrosymmetric, only the threefold symmetric surface of Bi₂Se₃ breaks inversion and twofold rotation symmetries and contributes to the LPGE, yielding a $\sin(3\phi + \phi_0)$ dependence of the LPGE current for a single domain under normal incidence (see the Supplemental Material [85] for derivations). Since the spot size of the NIR pump (order 1 mm) vastly exceeds the domain size of Bi₂Se₃ [order 1 μm ; see Figs. 3(c) and 3(d)], the THz emission method measures the net LPGE produced by a large ensemble of Bi₂Se₃ domains. Since twinned domains in the sample produce oppositely signed LPGE responses, as demonstrated in Fig. 1(b), the azimuthal dependence of the single domain LPGE can be generalized to the case of many

domains as $(f_+ - f_-) \sin(3\phi + \phi_0)$, where $f_+ + f_- = 1$ indicates the fraction of oppositely oriented domains, respectively [85]. The observation of a clear threefold LPGE signal from the Bi₂Se₃ therefore indicates the presence of a dominant domain orientation over millimeter length scales, such that $f_+ \neq f_-$.

As SHG is limited by the same symmetry considerations as LPGE and expected to be generated from the surface of Bi₂Se₃ [63–66], the THz-HG of the samples is measured via intense TDTTS [71] at room temperature as shown schematically in Fig. 2(a). Intense broadband, quasisingle cycle THz pulses are generated from LiNbO₃ via the tilted pulse front method [86–88] by pumping with linearly polarized, broadband 800 nm, 35 fs pulses with a repetition rate of 1 kHz. The generated intense THz pulses are collected, directed through the sample at a waist of order 1 mm, and focused onto a ZnTe crystal by a quartet of OAPs in 8f geometry. Prior to the sample, optical filters (F1) convert the broadband pulse into a narrow-band few cycle pulse centered at 0.5 THz (spectral width $\sim 20\%$). After transmitting through the sample, the resulting THz pulse is passed through optical filters (F2) to suppress the spectral weight of the 0.5 THz fundamental pulse and pass the frequency range around the harmonic to

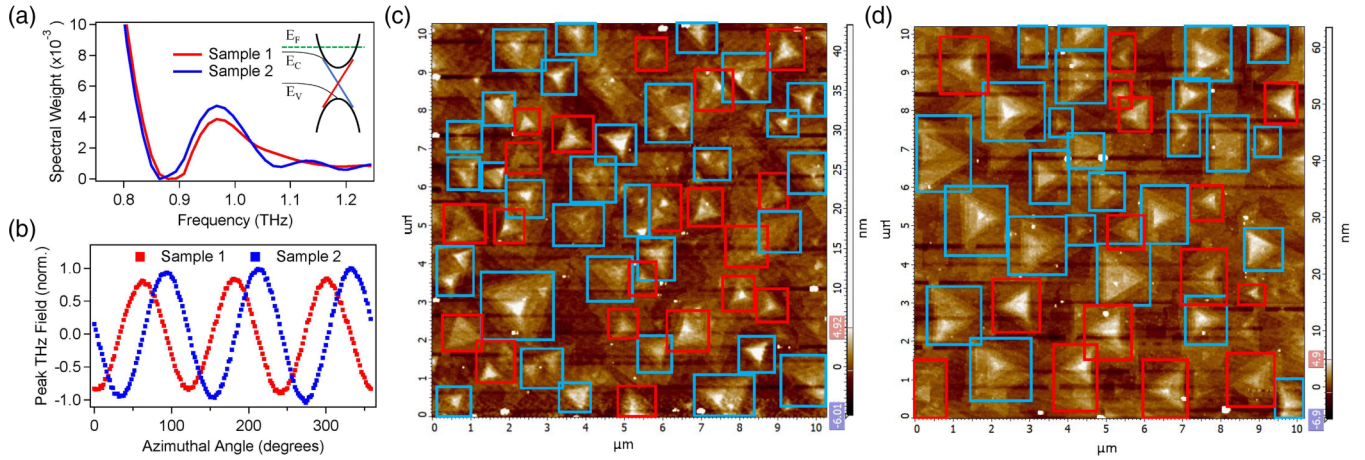


FIG. 3. (a), (b) Comparison of THz-SHG and LPGE, respectively, for two bare 100 QL Bi_2Se_3 samples. The band bending effect on the uncapped samples is sketched in the inset of (a), and the azimuthal angle in (b) is offset for clarity. (c), (d) Atomic force microscopy images of representative areas of bare 100 QL Bi_2Se_3 for sample 1 and sample 2, respectively, where oppositely oriented domains on the surface are highlighted with blue and red boxes.

be observed: 1.0 THz for SHG or 1.5 THz for THG. The remaining THz that impinges upon the ZnTe crystal is measured by standard electro-optic sampling [84], allowing the electric field profile to be mapped out in the time domain by varying the delay stage of the probe pulse. Finally, taking the Fourier transform of the THz pulse in the time domain yields the spectral weight of the pulse as a function of frequency.

The HG spectra for the Bi_2Se_3 samples shown in Fig. 2(b) exhibit clear THz-SHG at 1.0 THz and THz-THG at 1.5 THz when pumping with the 0.5 THz fundamental; however, no HG above the background level is observed for $(\text{Bi}_{0.9}\text{In}_{0.1})_2\text{Se}_3$. The common dip in the spectra at 1.4 THz is due to residual water absorption [89]. Such THz-HG has been attributed [39–47,67–69] to the ultrafast dynamics of Dirac fermions as they are accelerated by the THz light field through the surface Dirac cone. This Dirac fermion origin of the efficient THz-HG in the bismuth chalcogenides is confirmed here by direct comparison with the topologically trivial $(\text{Bi}_{0.9}\text{In}_{0.1})_2\text{Se}_3$ sample, where the THz-HG is dramatically reduced in the absence of Dirac fermions. Furthermore, three key features demonstrate strong agreement with the THz-THG observed in previous studies [42,46,47] of bismuth chalcogenides: First, the THG conversion efficiency is $\sim 0.04\%$ (accounting for the THG-specific filters), which closely matches the conversion efficiency in previous reports. Second, the yield of the THz-THG scales perturbatively as E_{pump}^3 , as shown in Fig. 2(c), which likewise agrees with previous results and contrasts sharply with the saturation observed in graphene [39–42] and Cd_3As_2 [43,44]. Third, the THz-THG yield is nearly thickness independent, as shown in Fig. 2(d), which is consistent with the dominant contribution to the THz-THG originating from the topological surface state. Together, these results reaffirm the conclusions of the previous studies, indicate that the intrinsic nonlinear properties of the Bi_2Se_3 samples measured here are consistent with those of the previous studies, and demonstrate the dominance of the surface Dirac fermions in the nonlinear THz response even when bulk contributions are not symmetry forbidden.

Returning to Fig. 2(b), a clear THz-SHG peak is observed at 1.0 THz for the Bi_2Se_3 samples, in addition to the THz-THG peak at 1.5 THz. As shown in Fig. 2(c), the 1.0 THz peak scales according to the E_{pump}^2 expectation for a perturbative second-order response (see [85] for comparison to linear fit). Furthermore, the 1.0 THz peak is thickness independent, as shown in Fig. 2(d), matching the expectation for Bi_2Se_3 where only the surface breaks inversion symmetry and twofold rotation symmetry as required for a second-order process. Since bulk contributions are symmetry forbidden [63–66], the band bending contribution is suppressed by the Se capping layer [78] [sketched in the inset of Fig. 2(b)] irrespective of the sample topology, Dirac fermions are known to dominate the nonlinear THz response when present [39–47,67–69], and no THz-SHG is observed from the topologically trivial Se-capped $(\text{Bi}_{0.9}\text{In}_{0.1})_2\text{Se}_3$, this clear THz-SHG response from Bi_2Se_3 can be attributed to the topological surface state. While both the THz-SHG and THz-THG originate from the topological surface state, the yield of twinned domains cancels for THz-SHG according to $(f_+ - f_-)$ whereas the yield adds for THz-THG according to $(f_+ + f_-)$. Thus, the lower THz-SHG yield compared to THz-THG in Fig. 2 accords with the theoretical expectation that twinned domains suppress the THz-SHG. This observation of THz-SHG reaching a high conversion efficiency of $\sim 0.005\%$ (accounting for the SHG-specific filters) is consistent with HG studies outside of the THz regime [63–69], but contrasts sharply with the previous THz studies [42,46,47] of bismuth chalcogenides, which failed to report THz-SHG.

Finally, we verify these conclusions by measuring capless Bi_2Se_3 samples. Figures 3(a) and 3(b), respectively, compare the THz-SHG and THz emission results for two 100 QL bare Bi_2Se_3 samples taken from the same batch to ensure similar growth quality, with both samples exposed to atmosphere for a similar duration of several hours to ensure stable and comparable $\chi_{\text{eff}}^{(2)}$ due to band bending [63,65,67,77,80] [sketched in the inset of Fig. 3(a)]. The capless samples exhibit no enhancement of either LPGE or THz-SHG compared to the

Se-capped samples, confirming that the band bending contribution is small and that the large second-order nonlinear response in Bi_2Se_3 is indeed due to the Dirac fermions.

The lack of a cap permits the orientation of surface domains to be determined by atomic force microscopy (AFM). Various points on the samples were therefore measured by AFM to verify the presence of unequal populations of twinned domains. Figures 3(c) and 3(d), respectively, display representative AFM images with twinned domains clearly visible on the surface of both samples. As variations in domain size and quality average out over many domains, the ratio of many domains yields a rough but sufficiently accurate proxy for comparing the relative populations of oppositely oriented domains. A careful counting of these domains shows that the ratio of oppositely oriented domains is $\sim 1.5 : 1$ in sample 1 and $\sim 1.8 : 1$ in sample 2, demonstrating that both samples have unequal (not $1 : 1$) populations of twinned domains. These domain ratios correlate with the magnitude of the second-order responses for the samples, agreeing with the theoretical expectation and confirming the dependence of both LPGE and THz-SHG upon the presence of unequal populations of twinned domains. This dependence of the second-order processes upon unequal populations of twinned domains presents one potential reason why the previous studies [42,46,47] of bismuth chalcogenides failed to report THz-SHG, and it highlights the importance of improving control over crystal growth for materials that break various symmetries.

To summarize, we have observed THz-SHG from the topological surface state of Bi_2Se_3 featuring a highly efficient conversion rate of $\sim 0.005\%$ and have proposed a plausible reason for the failure to observe THz-SHG in previous studies [42,46,47] of similar bismuth chalcogenides, namely the suppression of second-order processes by twinned domains [42,46,47]. By demonstrating intrinsic SHG in the THz regime for an equilibrium system, these results open a new nonlinear pathway to experimentally probing intraband quantum geometry via THz-HG methods. This crucial experimental advance motivates the extensive theoretical elaboration of nonlinear intraband quantum processes, as has

been accomplished for the interband [56], and enables further development of THz-HG techniques to discriminate between various nonlinear quantum effects. While various scattering [51–53] and quantum geometry [90–94] contributions to intraband nonlinear Hall effect involving Dirac fermions have been proposed, a full treatment of intraband SHG is lacking [52] and remains for future theoretical work. As the experimental capacity to probe intraband SHG in the THz regime has now been demonstrated, developing such theoretical models is the primary extant barrier to the unexplored frontier of nonlinear intraband quantum processes. Altogether, these results vastly expand the range of future studies by unlocking even-order HG in the THz regime and open new experimental and theoretical pathways to the low-energy study of topological surface states and nonlinear intraband quantum processes in noncentrosymmetric topological semimetals and twisted material systems in order to study the quantum geometrical effects.

ACKNOWLEDGMENTS

We thank F. de Juan, A. Grushin, T. Morimoto, and J. Lu for helpful discussions. J.S. was initially sponsored by the Army Research Office under the YIP award to L.W. under Grant No. W911NF-19-1-0342 (completed in 2022), and was partially supported by the Gordon and Betty Moore Foundation EPiQS Initiative under Grant GBMF9212 to L.W. (completed in 2023), and is supported by the Dissertation Completion Fellowship at the University of Pennsylvania. X.H. is supported by the NSF EPM program under Grant No. DMR-2213891. Z.N. acknowledges support from the Dissertation Completion Fellowship at the University of Pennsylvania. The work at Rutgers by X.Y., X.Y., D.M., A.G., and S.O. were supported by the Army Research Office under Grant No. W911NF-20-2-0166 and the center for Quantum Materials Synthesis (cQMS), funded by the Gordon and Betty Moore Foundation EPiQS initiative through Grant GBMF10104. L.W. acknowledges the support by Air Force Office of Scientific Research under Award No. FA955022-1-0410.

-
- [1] P. A. Franken, A. E. Hill, C. W. Peters, and G. Weinreich, Generation of optical harmonics, *Phys. Rev. Lett.* **7**, 118 (1961).
 - [2] Z. Ni, A. V. Haglund, B. Wang, H. and Xu, C. Bernhard, D. G. Mandrus, X. Qian, E. J. Mele, C. L. Kane, and L. Wu, Imaging the néel vector switching in the monolayer antiferromagnet MnPS_3 with strain-controlled Ising order, *Nat. Nanotechnol.* **16**, 782 (2021).
 - [3] Z. Ni, H. Zhang, D. A. Hopper, A. V. Haglund, N. Huang, D. Jariwala, L. C. Bassett, D. G. Mandrus, E. J. Mele, C. L. Kane, and L. Wu, Direct imaging of antiferromagnetic domains and anomalous layer-dependent mirror symmetry breaking in atomically thin MnPS_3 , *Phys. Rev. Lett.* **127**, 187201 (2021).
 - [4] T. T. Luu, M. Garg, S. Y. Kruchinin, A. Moulet, M. T. Hassan, and E. Goulielmakis, Extreme ultraviolet high-harmonic spectroscopy of solids, *Nature (London)* **521**, 498 (2015).
 - [5] J. Li, J. Lu, A. Chew, S. Han, J. Li, Y. Wu, H. Wang, S. Ghimire, and Z. Chang, Attosecond science based on high harmonic generation from gases and solids, *Nat. Commun.* **11**, 2748 (2020).
 - [6] M. Tonouchi, Cutting-edge terahertz technology, *Nat. Photon.* **1**, 97 (2007).
 - [7] M. C. Hoffmann and J. A. Fülöp, Intense ultrashort terahertz pulses: Generation and applications, *J. Phys. D* **44**, 083001 (2011).
 - [8] H. A. Hafez, X. Chai, A. Ibrahim, S. Mondal, D. Férachou, X. Ropagnol, and T. Ozaki, Intense terahertz radiation and their applications, *J. Opt.* **18**, 093004 (2016).
 - [9] R. Matsunaga, N. Tsuji, H. Fujita, A. Sugioka, K. Makise, Y. Uzawa, H. Terai, Z. Wang, H. Aoki, and R. Shimano, Light-induced collective pseudospin precession resonating with Higgs mode in a superconductor, *Science* **345**, 1145 (2014).

- [10] R. Matsunaga, Y. I. Hamada, K. Makise, Y. Uzawa, H. Terai, Z. Wang, and R. Shimano, Higgs amplitude mode in the BCS superconductors $\text{Nb}_{1-x}\text{Ti}_x\text{N}$ induced by terahertz pulse excitation, *Phys. Rev. Lett.* **111**, 057002 (2013).
- [11] N. Tsuji and H. Aoki, Theory of anderson pseudospin resonance with higgs mode in superconductors, *Phys. Rev. B* **92**, 064508 (2015).
- [12] D. Pekker and C. Varma, Amplitude/Higgs modes in condensed matter physics, *Annu. Rev. Condens. Matter Phys.* **6**, 269 (2015).
- [13] R. Shimano and N. Tsuji, Higgs mode in superconductors, *Annu. Rev. Condens. Matter Phys.* **11**, 103 (2020).
- [14] T. Cea, C. Castellani, and L. Benfatto, Nonlinear optical effects and third-harmonic generation in superconductors: Cooper pairs versus Higgs mode contribution, *Phys. Rev. B* **93**, 180507(R) (2016).
- [15] N. Tsuji, Y. Murakami, and H. Aoki, Nonlinear light–Higgs coupling in superconductors beyond BCS: Effects of the retarded phonon-mediated interaction, *Phys. Rev. B* **94**, 224519 (2016).
- [16] R. Matsunaga, N. Tsuji, K. Makise, H. Terai, H. Aoki, and R. Shimano, Polarization-resolved terahertz third-harmonic generation in a single-crystal superconductor NbN: Dominance of the Higgs mode beyond the BCS approximation, *Phys. Rev. B* **96**, 020505(R) (2017).
- [17] A. Moor, A. F. Volkov, and K. B. Efetov, Amplitude higgs mode and admittance in superconductors with a moving Condensate, *Phys. Rev. Lett.* **118**, 047001 (2017).
- [18] X. Yang, C. Vaswani, C. Sundahl, M. Mootz, P. Gagel, L. Luo, J. H. Kang, P. P. Orth, I. E. Perakis, C. B. Eom, and J. Wang, Terahertz-light quantum tuning of a metastable emergent phase hidden by superconductivity, *Nat. Mater.* **17**, 586 (2018).
- [19] X. Yang, C. Vaswani, C. Sundahl, M. Mootz, L. Luo, J. H. Kang, I. E. Perakis, C. B. Eom, and J. Wang, Lightwave-driven gapless superconductivity and forbidden quantum beats by terahertz symmetry breaking, *Nat. Photon.* **13**, 707 (2019).
- [20] S. Nakamura, Y. Iida, Y. Murotani, R. Matsunaga, H. Terai, and R. Shimano, Infrared activation of the higgs mode by supercurrent injection in superconducting NbN, *Phys. Rev. Lett.* **122**, 257001 (2019).
- [21] G. Seibold, M. Udina, C. Castellani, and L. Benfatto, Third harmonic generation from collective modes in disordered superconductors, *Phys. Rev. B* **103**, 014512 (2021).
- [22] L. Schwarz, R. Haenel, and D. Manske, Phase signatures in the third-harmonic response of Higgs and coexisting modes in superconductors, *Phys. Rev. B* **104**, 174508 (2021).
- [23] L. Luo, M. Mootz, J. H. Kang, C. Huang, K. Eom, J. W. Lee, C. Vaswani, Y. G. Collantes, E. E. Hellstrom, I. E. Perakis, C. B. Eom, and J. Wang, Quantum coherence tomography of light-controlled superconductivity, *Nat. Phys.* **19**, 201 (2022).
- [24] J. Yuan, L. Shi, L. Yue, B. Li, Z. Wang, S. Xu, T. Xu, Y. Wang, Z. Gan, F. Chen, Z. Lin, X. Wang, K. Jin, X. Wang, J. Luo, S. Zhang, Q. Wu, Q. Liu, T. Hu, R. Li *et al.*, Dynamical interplay between superconductivity and pseudogap in cuprates as revealed by terahertz third-harmonic generation spectroscopy, *Sci. Adv.* **10**, eadg9211 (2024).
- [25] L. Feng, J. Cao, T. Priessnitz, Y. Dai, T. de Oliveira, J. Yuan, R. Oka, M.-J. Kim, M. Chen, A. N. Ponomaryov, I. Ilyakov, H. Zhang, Y. Lv, V. Mazzotti, G. Kim, G. Christiani, G. Logvenov, D. Wu, Y. Huang, J.-C. Deinert *et al.*, Dynamical interplay between superconductivity and charge density waves: A nonlinear terahertz study of coherently driven $2H\text{-NbSe}_2$, *Phys. Rev. B* **108**, L100504 (2023).
- [26] K. Kaj, K. A. Cremin, I. Hammock, J. Schalch, D. N. Basov, and R. D. Averitt, Terahertz third harmonic generation in c -axis $\text{La}_{1.85}\text{Sr}_{0.15}\text{CuO}_4$, *Phys. Rev. B* **107**, L140504 (2023).
- [27] H. Chu, S. Kovalev, Z. X. Wang, L. Schwarz, T. Dong, L. Feng, R. Haenel, M.-J. Kim, P. Shabestari, L. P. Hoang, K. Honasoge, R. D. Dawson, D. Putzky, G. Kim, M. Puviani, M. Chen, N. Awari, A. N. Ponomaryov, I. Ilyakov, M. Bluschke *et al.*, Fano interference between collective modes in cuprate high-Tc superconductors, *Nat. Commun.* **14**, 1343 (2023).
- [28] S. Kovalev, T. Dong, L.-Y. Shi, C. Reinhoffer, T.-Q. Xu, H.-Z. Wang, Y. Wang, Z.-Z. Gan, S. Germanskiy, J.-C. Deinert, I. Ilyakov, P. H. M. van Loosdrecht, D. Wu, N.-L. Wang, J. Demsar, and Z. Wang, Band-selective third-harmonic generation in superconducting MgB_2 : Possible evidence for the Higgs amplitude mode in the dirty limit, *Phys. Rev. B* **104**, L140505 (2021).
- [29] C. Reinhoffer, P. Pilch, A. Reinold, P. Derendorf, S. Kovalev, J.-C. Deinert, I. Ilyakov, A. Ponomaryov, M. Chen, T.-Q. Xu, Y. Wang, Z.-Z. Gan, D.-S. Wu, J.-L. Luo, S. Germanskiy, E. A. Mashkovich, P. H. M. van Loosdrecht, I. M. Eremin, and Z. Wang, High-order nonlinear terahertz probing of the two-band superconductor MgB_2 : Third- and fifth-order harmonic generation, *Phys. Rev. B* **106**, 214514 (2022).
- [30] K. Isoyama, N. Yoshikawa, K. Katsumi, J. Wong, N. Shikama, Y. Sakishita, F. Nabeshima, A. Maeda, and R. Shimano, Light-induced enhancement of superconductivity in iron-based superconductor $\text{FeSe}_{0.5}\text{Te}_{0.5}$, *Commun. Phys.* **4**, 160 (2021).
- [31] C. Vaswani, J. H. Kang, M. Mootz, L. Luo, X. Yang, C. Sundahl, D. Cheng, C. Huang, R. H. J. Kim, Z. Liu, Y. G. Collantes, E. E. Hellstrom, I. E. Perakis, C. B. Eom, and J. Wang, Light quantum control of persisting Higgs modes in iron-based superconductors, *Nat. Commun.* **12**, 258 (2021).
- [32] S. Rajasekaran, J. Okamoto, L. Mathey, M. Fechner, V. Thampy, G. D. Gu, and A. Cavalleri, Probing optically silent superfluid stripes in cuprates, *Science* **359**, 575 (2018).
- [33] H. Chu, M.-J. Kim, K. Katsumi, S. Kovalev, R. D. Dawson, L. Schwarz, N. Yoshikawa, G. Kim, D. Putzky, Z. Z. Li, H. Raffy, S. Germanskiy, J.-C. Deinert, N. Awari, I. Ilyakov, B. Green, M. Chen, M. Bawatna, G. Cristiani, G. Logvenov *et al.*, Phase-resolved Higgs response in superconducting cuprates, *Nat. Commun.* **11**, 1793 (2020).
- [34] K. Katsumi, M. Nishida, S. Kaiser, S. Miyasaka, S. Tajima, and R. Shimano, Near-infrared light-induced superconducting-like state in underdoped $\text{YBa}_2\text{Cu}_3\text{O}_y$ studied by c -axis terahertz third-harmonic generation, *Phys. Rev. B* **107**, 214506 (2023).
- [35] L. Schwarz and D. Manske, Theory of driven Higgs oscillations and third-harmonic generation in unconventional superconductors, *Phys. Rev. B* **101**, 184519 (2020).
- [36] F. Meng, M. D. Thomson, Q. ul Islam, B. Klug, A. Pashkin, H. Schneider, and H. G. Roskos, Intracavity third-harmonic generation in Si:B pumped by intense terahertz pulses, *Phys. Rev. B* **102**, 075205 (2020).
- [37] F. Meng, F. Walla, Q. ul Islam, A. Pashkin, H. Schneider, C. Jungemann, M. D. Thomson, and H. G. Roskos, Importance of

- valence-band anharmonicity and carrier distribution for third- and fifth-harmonic generation in Si:B pumped with intense terahertz pulses, *Phys. Rev. B* **106**, 075203 (2022).
- [38] F. Meng, F. Walla, S. Kovalev, J.-C. Deinert, I. Ilyakov, M. Chen, A. Ponomaryov, S. G. Pavlov, H.-W. Hübers, N. V. Abrosimov, C. Jungemann, H. G. Roskos, and M. D. Thomson, Higher-harmonic generation in boron-doped silicon from band carriers and bound-dopant photoionization, *Phys. Rev. Res.* **5**, 043141 (2023).
- [39] H. A. Hafez, S. Kovalev, J.-C. Deinert, Z. Mics, B. Green, N. Awari, M. Chen, S. Germanskiy, U. Lehnert, J. Teichert, Z. Wang, K.-J. Tielrooij, Z. Liu, Z. Chen, A. Narita, K. Müllen, M. Bonn, M. Gensch, and D. Turchinovich, Extremely efficient terahertz high-harmonic generation in graphene by hot Dirac fermions, *Nature (London)* **561**, 507 (2018).
- [40] S. Kovalev, H. A. Hafez, K.-J. Tielrooij, J.-C. Deinert, I. Ilyakov, N. Awari, D. Alcaraz, K. Soundarapandian, D. Saleta, S. Germanskiy, M. Chen, M. Bawatna, B. Green, F. H. L. Koppens, M. Mittendorff, M. Bonn, M. Gensch, and D. Turchinovich, Electrical tunability of terahertz nonlinearity in graphene, *Sci. Adv.* **7**, eabf9809 (2021).
- [41] J.-C. Deinert, D. Alcaraz Iranzo, R. Pérez, X. Jia, H. A. Hafez, I. Ilyakov, N. Awari, M. Chen, M. Bawatna, A. N. Ponomaryov, S. Germanskiy, M. Bonn, F. H. Koppens, D. Turchinovich, M. Gensch, S. Kovalev, and K.-J. Tielrooij, Grating-graphene metamaterial as a platform for terahertz nonlinear photonics, *ACS Nano* **15**, 1145 (2021).
- [42] K.-J. Tielrooij, A. Principi, D. S. Reig, A. Block, S. Varghese, S. Schreyeck, K. Brunner, G. Karczewski, I. Ilyakov, O. Ponomaryov, T. V. A. G. de Oliveira, M. Chen, J.-C. Deinert, C. G. Carbonell, S. O. Valenzuela, L. W. Molenkamp, T. Kiessling, G. V. Astakhov, and S. Kovalev, Milliwatt terahertz harmonic generation from topological insulator metamaterials, *Light: Sci. Appl.* **11**, 315 (2022).
- [43] B. Cheng, N. Kanda, T. N. Ikeda, T. Matsuda, P. Xia, T. Schumann, S. Stemmer, J. Itatani, N. P. Armitage, and R. Matsunaga, Efficient terahertz harmonic generation with coherent acceleration of electrons in the dirac semimetal Cd_3As_2 , *Phys. Rev. Lett.* **124**, 117402 (2020).
- [44] S. Kovalev, R. M. A. Dantas, S. Germanskiy, J.-C. Deinert, B. Green, I. Ilyakov, N. Awari, M. Chen, M. Bawatna, J. Ling, F. Xiu, P. H. M. van Loosdrecht, P. Surówka, T. Oka, and Z. Wang, Non-perturbative terahertz high-harmonic generation in the three-dimensional Dirac semimetal Cd_3As_2 , *Nat. Commun.* **11**, 2451 (2020).
- [45] S. Germanskiy, R. M. A. Dantas, S. Kovalev, C. Reinhoffer, E. A. Mashkovich, P. H. M. van Loosdrecht, Y. Yang, F. Xiu, P. Surówka, R. Moessner, T. Oka, and Z. Wang, Ellipticity control of terahertz high-harmonic generation in a Dirac semimetal, *Phys. Rev. B* **106**, L081127 (2022).
- [46] F. Giorgianni, E. Chiadroni, A. Rovere, M. Cestelli-Guidi, A. Perucchi, M. Bellaveglia, M. Castellano, D. Di Giovenale, G. Di Pirro, M. Ferrario, R. Pompili, C. Vaccarezza, F. Villa, A. Cianchi, A. Mostacci, M. Petrarca, M. Brahlek, N. Koirala, S. Oh, and S. Lupi, Strong nonlinear terahertz response induced by dirac surface states in Bi_2Se_3 topological insulator, *Nat. Commun.* **7**, 11421 (2016).
- [47] S. Kovalev, K.-J. Tielrooij, J.-C. Deinert, I. Ilyakov, N. Awari, M. Chen, A. Ponomaryov, M. Bawatna, T. V. A. G. de Oliveira, L. M. Eng, K. A. Kuznetsov, D. A. Safronenkov, G. K. Kitaeva, P. I. Kuznetsov, H. A. Hafez, D. Turchinovich, and M. Gensch, Terahertz signatures of ultrafast Dirac fermion relaxation at the surface of topological insulators, *npj Quantum Mater.* **6**, 84 (2021).
- [48] C. Vaswani, M. Mootz, C. Sundahl, D. H. Mudiyansele, J. H. Kang, X. Yang, D. Cheng, C. Huang, R. H. J. Kim, Z. Liu, L. Luo, I. E. Perakis, C. B. Eom, and J. Wang, Terahertz second-harmonic generation from lightwave acceleration of symmetry-breaking nonlinear supercurrents, *Phys. Rev. Lett.* **124**, 207003 (2020).
- [49] S. Nakamura, K. Katsumi, H. Terai, and R. Shimano, Nonreciprocal terahertz second-harmonic generation in superconducting NbN under supercurrent injection, *Phys. Rev. Lett.* **125**, 097004 (2020).
- [50] K. Lee, J. Park, B. J. Kang, W. T. Kim, H.-D. Kim, S. Baek, K. J. Ahn, B. Min, and F. Rotermund, Electrically controllable terahertz second-harmonic generation in GaAs, *Adv. Opt. Mater.* **8**, 2000359 (2020).
- [51] V. I. Belinicher and B. I. Sturman, The photogalvanic effect in media lacking a center of symmetry, *Soviet Physics Uspekhi* **23**, 199 (1980).
- [52] H. Isobe, S.-Y. Xu, and L. Fu, High-frequency rectification via chiral Bloch electrons, *Sci. Adv.* **6**, eaay2497 (2020).
- [53] P. He, G. K. W. Koon, H. Isobe, J. Y. Tan, J. Hu, A. H. C. Neto, L. Fu, and H. Yang, Graphene moiré superlattices with giant quantum nonlinearity of chiral Bloch electrons, *Nat. Nanotechnol.* **17**, 378 (2022).
- [54] T. Morimoto and N. Nagaosa, Topological nature of nonlinear optical effects in solids, *Sci. Adv.* **2**, e1501524 (2016).
- [55] L. Wu, S. Patankar, T. Morimoto, N. L. Nair, E. Thewalt, A. Little, J. G. Analytis, J. E. Moore, and J. Orenstein, Giant anisotropic nonlinear optical response in transition metal monopnictide Weyl semimetals, *Nat. Phys.* **13**, 350 (2017).
- [56] Q. Ma, A. G. Grushin, and K. S. Burch, Topology and geometry under the nonlinear electromagnetic spotlight, *Nat. Mater.* **20**, 1601 (2021).
- [57] E. J. König, H.-Y. Xie, D. A. Pesin, and A. Levchenko, Photogalvanic effect in Weyl semimetals, *Phys. Rev. B* **96**, 075123 (2017).
- [58] O. Matsyshyn and I. Sodemann, Nonlinear hall acceleration and the quantum rectification sum rule, *Phys. Rev. Lett.* **123**, 246602 (2019).
- [59] R. Valdés Aguilar, A. V. Stier, W. Liu, L. S. Bilbro, D. K. George, N. Bansal, L. Wu, J. Cerne, A. G. Markelz, S. Oh, and N. P. Armitage, Terahertz response and colossal kerr rotation from the surface states of the topological insulator Bi_2Se_3 , *Phys. Rev. Lett.* **108**, 087403 (2012).
- [60] L. Wu, M. Brahlek, R. Valdés Aguilar, A. V. Stier, C. M. Morris, Y. Lubashevsky, L. S. Bilbro, N. Bansal, S. Oh, and N. P. Armitage, A sudden collapse in the transport lifetime across the topological phase transition in $(\text{Bi}_{1-x}\text{In}_x)_2\text{Se}_3$, *Nat. Phys.* **9**, 410 (2013).
- [61] L. Wu, W.-K. Tse, M. Brahlek, C. M. Morris, R. V. Aguilar, N. Koirala, S. Oh, and N. P. Armitage, High-resolution faraday rotation and electron-phonon coupling in surface states of the bulk-insulating topological insulator $\text{Cu}_{0.02}\text{Bi}_2\text{Se}_3$, *Phys. Rev. Lett.* **115**, 217602 (2015).
- [62] L. Wu, M. Salehi, N. Koirala, J. Moon, S. Oh, and N. P. Armitage, Quantized faraday and kerr rotation and axion

- electrodynamics of a 3D topological insulator, *Science* **354**, 1124 (2016).
- [63] D. Hsieh, J. W. McIver, D. H. Torchinsky, D. R. Gardner, Y. S. Lee, and N. Gedik, Nonlinear optical probe of tunable surface electrons on a topological insulator, *Phys. Rev. Lett.* **106**, 057401 (2011).
- [64] D. Hsieh, F. Mahmood, J. W. McIver, D. R. Gardner, Y. S. Lee, and N. Gedik, Selective probing of photoinduced charge and spin dynamics in the bulk and surface of a topological insulator, *Phys. Rev. Lett.* **107**, 077401 (2011).
- [65] J. W. McIver, D. Hsieh, S. G. Drapcho, D. H. Torchinsky, D. R. Gardner, Y. S. Lee, and N. Gedik, Theoretical and experimental study of second harmonic generation from the surface of the topological insulator Bi_2Se_3 , *Phys. Rev. B* **86**, 035327 (2012).
- [66] V. Mizrahi and J. E. Sipe, Phenomenological treatment of surface second-harmonic generation, *J. Opt. Soc. Am. B* **5**, 660 (1988).
- [67] Y. Bai, F. Fei, S. Wang, N. Li, X. Li, F. Song, R. Li, Z. Xu, and P. Liu, High-harmonic generation from topological surface states, *Nat. Phys.* **17**, 311 (2021).
- [68] C. P. Schmid, L. Weigl, P. Grössing, V. Junk, C. Gorini, S. Schlauderer, S. Ito, M. Meierhofer, N. Hofmann, D. Afanasiev, J. Crewse, K. A. Kokh, O. E. Tereshchenko, J. Gütde, F. Evers, J. Wilhelm, K. Richter, U. Höfer, and R. Huber, Tunable non-integer high-harmonic generation in a topological insulator, *Nature (London)* **593**, 385 (2021).
- [69] C. Heide, Y. Kobayashi, D. R. Baykusheva, D. Jain, J. A. Sobota, M. Hashimoto, P. S. Kirchmann, S. Oh, T. F. Heinz, D. A. Reis, and S. Ghimire, Probing topological phase transitions using high-harmonic generation, *Nat. Photon.* **16**, 620 (2022).
- [70] T. Kampfrath, M. Battiato, P. Maldonado, G. Eilers, J. Nötzold, S. Mährlein, V. Zbarsky, F. Freimuth, Y. Mokrousov, S. Blügel, M. Wolf, I. Radu, P. M. Oppeneer, and M. Münzenberg, Terahertz spin current pulses controlled by magnetic heterostructures, *Nat. Nanotechnol.* **8**, 256 (2013).
- [71] M. C. Nuss and J. Orenstein, Terahertz time-domain spectroscopy, in *Millimeter and Submillimeter Wave Spectroscopy of Solids*, edited by G. Grüner (Springer, Heidelberg, 1998), pp. 7–50.
- [72] N. Bansal, Y. S. Kim, E. Edrey, M. Brahlek, Y. Horibe, K. Iida, M. Tanimura, G.-H. Li, T. Feng, H.-D. Lee, T. Gustafsson, E. Andrei, and S. Oh, Epitaxial growth of topological insulator Bi_2Se_3 film on Si(111) with atomically sharp interface, *Thin Solid Films* **520**, 224 (2011).
- [73] N. Bansal, Y. S. Kim, M. Brahlek, E. Edrey, and S. Oh, Thickness-independent transport channels in topological insulator Bi_2Se_3 thin films, *Phys. Rev. Lett.* **109**, 116804 (2012).
- [74] D. Hsieh, Y. Xia, D. Qian, L. Wray, F. Meier, J. H. Dil, J. Osterwalder, L. Patthey, A. V. Fedorov, H. Lin, A. Bansil, D. Grauer, Y. S. Hor, R. J. Cava, and M. Z. Hasan, Observation of time-reversal-protected single-dirac-cone topological-insulator states in Bi_2Te_3 and Sb_2Te_3 , *Phys. Rev. Lett.* **103**, 146401 (2009).
- [75] M. Brahlek, Y. S. Kim, N. Bansal, E. Edrey, and S. Oh, Surface versus bulk state in topological insulator Bi_2Se_3 under environmental disorder, *Appl. Phys. Lett.* **99**, 012109 (2011).
- [76] R. Valdés Aguilar, L. Wu, A. V. Stier, L. S. Bilbro, M. Brahlek, N. Bansal, S. Oh, and N. P. Armitage, Aging and reduced bulk conductance in thin films of the topological insulator Bi_2Se_3 , *J. Appl. Phys.* **113**, 153702 (2013).
- [77] L.-G. Zhu, B. Kubera, K. Fai Mak, and J. Shan, Effect of surface states on terahertz emission from the Bi_2Se_3 Surface, *Sci. Rep.* **5**, 10308 (2015).
- [78] M. Salehi, M. Brahlek, N. Koirala, J. Moon, L. Wu, N. P. Armitage, and S. Oh, Stability of low-carrier-density topological-insulator Bi_2Se_3 thin films and effect of capping layers, *APL Mater.* **3**, 091101 (2015).
- [79] J. W. McIver, D. Hsieh, H. Steinberg, P. Jarillo-Herrero, and N. Gedik, Control over topological insulator photocurrents with light polarization, *Nat. Nanotechnol.* **7**, 96 (2012).
- [80] L. Braun, G. Mussler, A. Hruban, M. Konczykowski, T. Schumann, M. Wolf, M. Münzenberg, L. Perfetti, and T. Kampfrath, Ultrafast photocurrents at the surface of the three-dimensional topological insulator Bi_2Se_3 , *Nat. Commun.* **7**, 13259 (2016).
- [81] P. Olbrich, L. E. Golub, T. Herrmann, S. N. Danilov, H. Plank, V. V. Bel'kov, G. Mussler, C. Weyrich, C. M. Schneider, J. Kampmeier, D. Grützmacher, L. Plucinski, M. Eschbach, and S. D. Ganichev, Room-temperature high-frequency transport of dirac fermions in epitaxially grown Sb_2Te_3 - and Bi_2Te_3 -Based Topological Insulators, *Phys. Rev. Lett.* **113**, 096601 (2014).
- [82] Z. Ni, B. Xu, M.-Á. Sánchez-Martínez, Y. Zhang, K. Manna, C. Bernhard, J. W. F. Venderbos, F. de Juan, C. Felser, A. G. Grushin, and L. Wu, Linear and nonlinear optical responses in the chiral multifold semimetal RhSi, *npj Quantum Mater.* **5**, 96 (2020).
- [83] Z. Ni, K. Wang, Y. Zhang, O. Pozo, B. Xu, X. Han, K. Manna, J. Paglione, C. Felser, A. G. Grushin, F. de Juan, E. J. Mele, and L. Wu, Giant topological longitudinal circular photo-galvanic effect in the chiral multifold semimetal CoSi, *Nat. Commun.* **12**, 154 (2021).
- [84] Q. Wu and X. Zhang, Ultrafast electrooptic field sensors, *Appl. Phys. Lett.* **68**, 1604 (1996).
- [85] See Supplemental Material at <http://link.aps.org/supplemental/10.1103/PhysRevB.109.245112> for a derivation of LPGE for the Bi_2Se_3 surface, the extension to many domains, and a fitting comparison for the THz-SHG.
- [86] J. Hebling, G. Almási, I. Z. Kozma, and J. Kuhl, Velocity matching by pulse front tilting for large-area THz-pulse generation, *Opt. Express* **10**, 1161 (2002).
- [87] J. A. Fülöp, L. Pálfalvi, G. Almási, and J. Hebling, Design of high-energy terahertz sources based on optical rectification, *Opt. Express* **18**, 12311 (2010).
- [88] M. Kunitski, M. Richter, M. D. Thomson, A. Vredenburg, J. Wu, T. Jahnke, M. Schöffler, H. Schmidt-Böcking, H. G. Roskos, and R. Dörner, Optimization of single-cycle terahertz generation in LiNbO_3 for sub-50 femtosecond pump pulses, *Opt. Express* **21**, 6826 (2013).
- [89] M. van Exter, C. Fattering, and D. Grischkowsky, Terahertz time-domain spectroscopy of water vapor, *Opt. Lett.* **14**, 1128 (1989).
- [90] Q. Ma, S.-Y. Xu, H. Shen, D. MacNeill, V. Fatemi, T.-R. Chang, A. M. Mier Valdivia, S. Wu, Z. Du, C.-H. Hsu, S. Fang, Q. D. Gibson, K. Watanabe, T. Taniguchi, R. J. Cava, E. Kaxiras, H.-Z. Lu, H. Lin, L. Fu, N. Gedik *et al.*, Observation of the nonlinear Hall effect under time-reversal-symmetric conditions, *Nature (London)* **565**, 337 (2019).

- [91] K. Kang, T. Li, E. Sohn, J. Shan, and K. F. Mak, Nonlinear anomalous Hall effect in few-layer WTe_2 , *Nat. Mater.* **18**, 324 (2019).
- [92] P. He, H. Isobe, D. Zhu, C.-H. Hsu, L. Fu, and H. Yang, Quantum frequency doubling in the topological insulator Bi_2Se_3 , *Nat. Commun.* **12**, 698 (2021).
- [93] A. Gao, Y.-F. Liu, J.-X. Qiu, B. Ghosh, T. V. Trevisan, Y. Onishi, C. Hu, T. Qian, H.-J. Tien, S.-W. Chen, M. Huang, D. Bérubé, H. Li, C. Tzschaschel, T. Dinh, Z. Sun, S.-C. Ho, S.-W. Lien, B. Singh, K. Watanabe *et al.*, Quantum metric nonlinear Hall effect in a topological antiferromagnetic heterostructure, *Science* **381**, 181 (2023).
- [94] N. Wang, D. Kaplan, Z. Zhang, T. Holder, N. Cao, A. Wang, X. Zhou, F. Zhou, Z. Jiang, C. Zhang, S. Ru, H. Cai, K. Watanabe, T. Taniguchi, B. Yan, and W. Gao, Quantum-metric-induced nonlinear transport in a topological antiferromagnet, *Nature (London)* **621**, 487 (2023).